Composites Part C: Open Access 11 (2023) 100354

Contents lists available at ScienceDirect

Composites Part C: Open Access

journal homepage: www.sciencedirect.com/journal/composites-part-c-open-access

Effect of aging on the in-plane and out-of-plane mechanical properties of composites for design of marine structures

A. Robin [a], M. Arhant [a], P. Davies [a,*], S. Lejeune [a], E. Lolive [b], T. Bonnemains [b], B. Habert [c]

[a] Advanced Structural Materials and Hyperbaric Testing Laboratory (SMASH), Ifremer, Centre de Bretagne, Plouzané, France
[b] Institut de Recherche Dupuy de Lôme (IRDL – UMR CNRS 6027), Université de Bretagne Occidentale (UBO), France
[c] Direction Générale de l'Armement (DGA), IP/MCM/PMA, Paris, France

ARTICLE INFO

Keywords:
Seawater
Saturation
Durability
Long term behavior

ABSTRACT

This paper describes an approach allowing aging to be included in the design of marine structures. Two types of aging are considered, physical aging and seawater saturation. The latter is shown to be more severe for this material, with losses in properties of up to 30% being measured after aging. A complete set of in-plane and out-of-plane properties was generated for a carbon/epoxy composite, and these were then used as input data to model the response of a flexural beam under a mixed shear/bending load. Reasonable agreement is found between model and test results; both show the strong influence of seawater conditioning on the composite performance, with a reduction in strength after aging of around 35%. This approach can be applied to account for seawater aging during the design of composite structures.

1. Introduction

Composite materials are now widely used in many applications, including the marine industry [1]. Historically, the first marine structures were developed immediately after the Second world war, when the US Navy built small personnel boats [2]. These glass fiber reinforced composite boats proved to be stiff, strong, durable and easy to repair, leading to a rapid expansion of composite use for US naval craft in the 1960's. Over the years, improvements to manufacturing techniques have resulted in widespread use of Fiber Reinforced Plastics (FRP), often replacing aluminum alloys [3]: this is due to advantages inherent to composite materials, including excellent specific material properties, resistance to corrosion, good fatigue performance and the ease with which they can be formed into complex shapes [4]. Today, FRPs are increasingly being adopted in marine structures, from oil platforms to underwater vehicles [2], and newer applications include ship superstructures, masts and propulsion systems. For high-performance applications, Carbon Fiber Reinforced Plastic (CRFP) is preferred, while glass fiber reinforced composites are being replaced by natural fibre composites in some boat structures.

A recent application of CFRP composites concerns propellers and turbine blades: this is a particularly demanding application, combining high stresses, long term loading and permanent seawater immersion [5,6]. The technical feasibility of using composites to replace metallic structures has been shown [7] but their mechanical behavior after prolonged water immersion is not yet well known. Historically, the first composite propellers and turbine blades were manufactured using a wet lay-up process [8]. An examination of the feasibility of manufacturing small marine propellers with Resin Transfer Molding (RTM) was discussed in [9], in order to reduce void content and material waste, combined with the ability to mold complex shapes. Hand lay-up is still sometimes used [10,11], but the processes used more commonly in the aeronautics industry are gradually being adopted, due to the high added value of these composite structures. One example is the use of carbon fiber prepreg to manufacture a five-blade propeller with a diameter of 250 mm, using the compression molding process [12]. The introduction of Automated Fiber Placement (AFP) is another promising alternative, and this has been shown to result in optimal mechanical properties of composite hydrofoils [13,14]. Studies on thermoplastic composite blades are also possible using this process. The geometry of these structures varies, but they all possess a small radius of curvature at the leading edge and variable thickness. The potential for out-of-plane loading is very high.

A feature of polymeric marine materials is the need to consider the effects of moisture in their design [15,16]. For these applications, the immersion of the composite component leads to migration of water into

* Corresponding author.
E-mail address: peter.davies@ifremer.fr (P. Davies).

https://doi.org/10.1016/j.jcomc.2023.100354
Received 27 December 2022; Accepted 8 March 2023
Available online 24 March 2023

Table 1
Information on panels manufactured.

Name	Layup	Mechanical test	Thickness [mm]	Fiber volume ratio [%]	Void content [%]	T_g [°C]
Unreinforced Epoxy	–	Tension [34] Shear [35]	2.3	–	< 1	74
Thin UD	$[0]_4$	Tension [36] Compression [37]	2.2	65	2.2	78
Thick UD	$[0]_{42}$	Out-of-plane shear [35]	23.1	67	9.0	82
Fracture toughness	$[0]_6$	Mode I [38] Mode II [39] Mixed-Mode Bending [40]	3.3	66	2.2	75
Biaxial	$[-45, 45]_S$	In-plane shear [41]	2.4	61	6	76
Quasi-isotropic (QI)	$[0, (-45, 45)_2, 90]_S$	Four point bending [42]	4.4	64	3.2	75

the composite, which is accelerated when temperature is raised. The consequences of water uptake have been extensively studied [17] but it is important to note that marine composites are often significantly thicker than aerospace composites [18] and the greater the thickness, the longer it takes to reach water saturation [15].

In order to evaluate seawater sensitivity most published studies use either flexural tests or in-plane loading. The former can be difficult to apply in predictive methods as they involve a complex loading state, while the latter are limited to investigations of simple geometries. An exception is the recent studies by Le Blanc, Shukla and colleagues, who have investigated the influence of environmental degradation on tubular composite structures [19–21]. They applied an accelerated aging procedure and used the Arrhenius equation to predict lifetime under static and dynamic external pressure loading for underwater applications. They also aged some samples under pressure [22]. Although flexural modulus of the carbon/epoxy composite dropped after aging in saline solution the influence on hydrostatic and blast performance was generally quite small for the conditions tested.

The loading of thick propellers will involve out-of-plane loads, so these should also be investigated in water aging studies. Direct test methods have been used in the past to determine out-of-plane mechanical properties of composites. Out-of-plane shear modulus can be obtained using the Iosipescu test configuration [23] and the V-notched configuration [24]. Determining shear strength with these tests is complex, since multiple cracks can appear in the notch tips area. Another test to determine the out-of-plane shear properties uses the Arcan fixture [25]. Through-thickness tensile and compressive modulus and strength can be obtained using the parallel waist block geometry developed by the UK Defense Evaluation and Research Agency (DERA) [26,27]. However, it requires composites with thickness up to 20 mm, and the authors pointed out that the materials tested showed a highly non-linear behavior.

Finally, the last aspect to consider is the composite fracture toughness. Several tests have been developed to characterize both interlaminar and translaminar crack initiation and propagation [28].

Previous studies have evaluated the influence of seawater aging on both quasi-static behavior [29,30] and fatigue performance [31] of CFRP. These studies focused on in-plane loadings, and it has been shown that the loss of mechanical properties with aging is increased when the role of the matrix become significant. For this reason, it is important to also study the influence of wet aging on out-of-plane properties, focusing on the properties which can be directly introduced into numerical codes. Some published studies have indicated that both epoxy and carbon/-epoxy fracture toughness are sensitive to moisture, particularly under shear loading [32,33].

The aim of the present study is to characterize and understand the influence of seawater aging on both in-plane and out-of-plane behavior of a C/Epoxy composite. First the materials and test methods are presented. Then in-plane and out-of-plane properties of as-received (dry) specimens are characterized, followed by similar tests on samples both physically aged and saturated in seawater. These sets of data are then introduced into a finite element (FE) model of a composite beam subjected to a combination of flexural and out-of-plane shear loading. This provides a prediction of beam behavior which is finally compared to test results on dry and saturated specimens.

2. Materials and methods

2.1. Materials and manufacturing process

In this study, an amine cured epoxy system from Sicomin (SR8100 + SD4772) has been examined. The carbon fiber reinforcement is a commercial product with improved infusion capabilities (T700). Two carbon fiber fabrics were used to manufacture the panels: UD fabrics with a mass per unit area of 600 g/m^2 and a biaxial fabric with a mass per unit area of 600 g/m^2 for plies oriented at ±45°.

First neat resin plates were produced, in order to characterize the matrix alone, by pouring liquid resin vertically between two aluminum plates separated by an all-around 3 mm thick spacer. Composite panels were then manufactured by infusion. Following the resin supplier's datasheet, the material was post-cured for 16 h at 60 °C. Because of the aging process after the post cure, and to be sure to have complete initial cross-linking, an additional cure step was performed at 120 °C for 2 h. After curing, samples were analyzed by DSC (differential scanning calorimetry) and a T_g of 78 °C ± 1 °C was obtained for both neat resin and composites.

To obtain both in-plane and out of plane properties of this material system, four types of composite panels were manufactured, Table 1. Void contents were measured from polished sections using ImageJ™ software and fiber volume ratio was measured by thermo-gravimetric analysis (TGA) under nitrogen. Aging was performed on the full panels, which were then cut to the coupon dimensions before testing. Manufacture of the 20 mm thick panel was less straightforward and showed higher void content but still allowed a high fiber volume ratio to be obtained.

2.2. Aging of coupons

Mechanical properties of composite materials are highly dependent on both the manufacturing process and the service environment. To investigate whether sea water aging has an effect on the mechanical properties of a given material system, specimens must be immersed until water saturation is reached. Immersing specimens in natural conditions, i.e. at low temperatures (typically between 4 and 25 °C for marine structures) involves very slow water diffusion kinetics, especially for thick specimens. Therefore, accelerated aging is usually performed, by increasing the water temperature. This allows water saturation to be reached more quickly.

For this study, pure resin coupons (50 × 50 × 3 mm^3) and QI coupons with a layup of ($[0,(-45,45)_2,90]_S$) and dimensions of 40 × 40 × 4.4 mm^3 were immersed in natural seawater at 60 °C in order to accelerate the diffusion of water into the material and to saturate faster. This temperature was chosen based on the dry glass transition of the material (78 °C). Indeed, to keep the material in the glassy state during aging, an

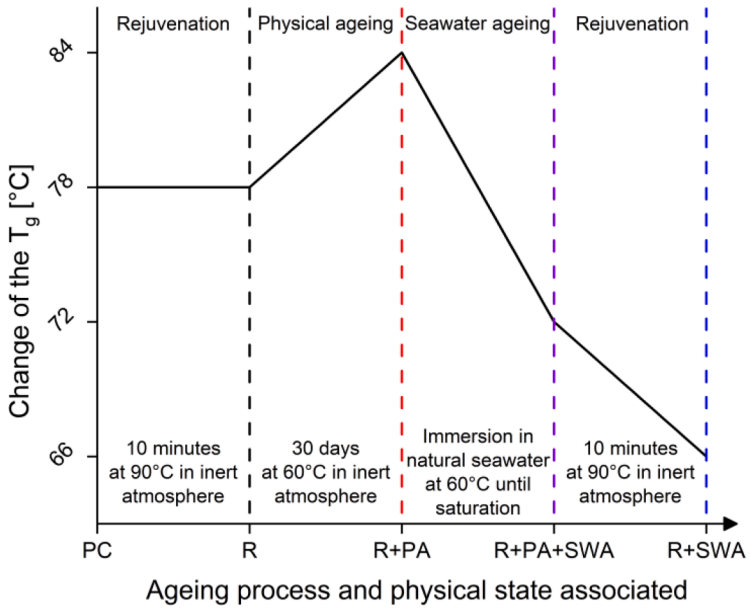

Fig. 1. Aging process used in this study to obtain rejuvenated, physically aged and seawater aged materials -PC (Post Cured), R (Rejuvenated), PA (Physical Aging) and SWA (Sea Water Aging).

aging temperature lower than the T_g must be used. Weighing was performed at different immersion times on three coupons per condition. The weight gain M(t) induced by water ingress is defined as follows, Eq. (1):

$$M(t) = \frac{m(t) - m_0}{m_0} \tag{1}$$

Where m(t) is the mass of the sample after a given aging time t and m_0 the dry mass of the sample before aging. Based on the weight gain measurements, the mass at saturation can be determined together with the diffusion coefficient determined following Eq. (2). A 1-D diffusion model supposing an isotropic diffusion in the material was also applied, based on Fick's law Eq. (3).

$$D = \frac{\pi}{16}\cdot\frac{h^2}{t}\cdot\left(\frac{M(t)}{M_\infty}\right)^2 \tag{2}$$

$$\frac{M(t)}{M_\infty} = 1 - \frac{8}{\pi^2}\sum_i \frac{1}{(2i+1)^2}\cdot\exp\left(-\frac{D(2i+1)^2\pi^2 t}{h^2}\right) \tag{3}$$

However, in some materials such as the one investigated in this work, physical aging (PA) can take place when the material evolves at a temperature close to its glass transition temperature, which is the case here (aging temperature of 60 °C and dry T_g of 78 °C). Physical aging is a reversible process accelerated by temperature observed in many studies on polymers [43,44]. When exposed to $T < T_g$, the macromolecular network of the epoxy relaxes progressively. This leads to an increase in T_g and some of the mechanical properties, such as the tensile modulus and failure stress [45]. However, when the material is subjected to $T > T_g$, this relaxation is removed, resulting in a new initial state known as 'rejuvenated' that can be assimilated to an unaged state.

This phenomenon is important to consider in this study because during accelerated aging in sea water, both the effects of water ingress and physical aging will contribute. In order to investigate these two effects individually, decoupling is necessary.

To do this, three different conditions were studied. First, the initial unaged state is considered as the rejuvenated state, i.e. after manufacture and post cure, so the material is placed for 10 min at 90 °C (above its T_g) in an inert atmosphere. This removes any thermal history that resulted from physical aging. Second, the material is placed in an oven at 60 °C for one month in an inert atmosphere. During this stage, physical aging takes place and induces an increase in the glass transition from 78 °C up to 84 °C. Testing after this step allows the effect of physical aging on the mechanical properties to be investigated. Finally, during sea water aging at 60 °C, both water ingress and physical aging occur. To investigate only the effect of water absorption on the mechanical properties after the sea water aging stage, the aged material is rejuvenated (placed for 10 min at 90 °C under inert atmosphere), which removes any thermal history (physical aging). However, the material is still fully saturated with water, so the water effect can be quantified.

A diagram representing the aging process and the associated physical states is shown in Fig. 1.

2.3. Mechanical properties

In order to perform a numerical simulation of the deformation of a composite structure, a stiffness matrix is required (Eq. (4)). Both in-plane and out-of-plane elastic properties are needed.

$$\begin{bmatrix}\varepsilon_{xx}\\ \varepsilon_{yy}\\ \varepsilon_{zz}\\ \varepsilon_{yz}\\ \varepsilon_{zx}\\ \varepsilon_{xy}\end{bmatrix} = \begin{bmatrix} \frac{1}{E_x} & \frac{-\nu_{yx}}{E_y} & \frac{-\nu_{zx}}{E_z} & 0 & 0 & 0\\ \frac{-\nu_{xy}}{E_x} & \frac{1}{E_y} & \frac{-\nu_{zy}}{E_z} & 0 & 0 & 0\\ \frac{-\nu_{xz}}{E_x} & \frac{-\nu_{yz}}{E_y} & \frac{1}{E_z} & 0 & 0 & 0\\ 0 & 0 & 0 & \frac{1}{2G_{yz}} & 0 & 0\\ 0 & 0 & 0 & 0 & \frac{1}{2G_{zx}} & 0\\ 0 & 0 & 0 & 0 & 0 & \frac{1}{2G_{xy}} \end{bmatrix} \begin{bmatrix}\sigma_{xx}\\ \sigma_{yy}\\ \sigma_{zz}\\ \sigma_{yz}\\ \sigma_{zx}\\ \sigma_{xy}\end{bmatrix} \tag{4}$$

In addition, if the failure of the structure is to be determined a set of failure properties corresponding to these different loading cases is necessary. A further aspect to consider is delamination.

An extensive experimental campaign was therefore carried out to obtain a complete set of data to predict the mechanical behavior of composite structures after aging. The section hereafter describes these different tests, first to characterize in-plane, then out-of-plane behavior.

$$\frac{G_I}{G_{II}} = \frac{3(e+L)^2}{3(e+L)^2 + 4(3e-L)^2} \quad \text{Eq. 8}$$

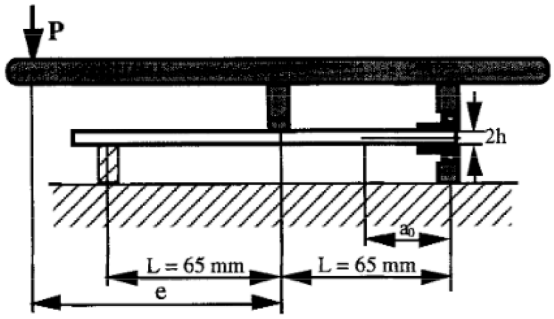

Fig. 2. MMB specimen (nominal measurements).

2.3.1. In plane properties

Tension tests. First, tension tests were performed on neat epoxy. This is not essential for the modeling but provides information on the matrix and is of interest to see how fiber reinforcements affect seawater aging. Prior to aging, coupons were cut using a CNC machine. The standard ISO 527-2 [34] with the coupon shape 1B was followed. Surfacing was used to avoid thickness variations. Second, tension tests were carried out on three composite orientations. The ISO 527–5 [36] standard was followed for tensile tests on 0° and 90°, while the ASTM D3518 [41] standard was followed for tensile tests at ±45°. Panels were cut using a wet diamond tipped saw. The dimensions of the specimens were 250 × 25 × 2.2 mm^3. Prior to the tests, 0/90/0 C/epoxy end tabs were bonded to the composite coupons to avoid premature failure in machine jaws. Tensile tests in the 0° direction were carried out using an Instron™ universal testing machine with a load cell of 200 kN, while other tensile tests were carried out using an Instron™ 5966 machine with a 10 kN load cell. All tensile tests were performed at 1 mm/min. Strain measurements were obtained by digital image correlation by applying a random graphite pattern on the specimen. Images were captured by a Basler™ camera at 2 frames per second and analyzed with the commercial Aramis GOM™ software.

Compression tests. Compression tests following the ASTM standard D6641 [37] were performed on 0° and 90° oriented coupons. This test, known as the combined loading compression (CLC) test method, was chosen to avoid failures from structural buckling. The loading-rate was fixed at 1 mm/min. C/Epoxy tapered end tabs with a lay-up of 0/90/0 were bonded on both sides of the coupon to avoid the crushing of the coupon near the compression platens. Strain gauges were bonded to both sides of the gage section of the sample to determine the buckling ratio which must be below 10% for a valid result. Five specimens per aging condition were tested for 0° and 90° oriented fibers, with a thickness of 2.15 mm. Coupons were cut with water jet to obtain good parallelism between the specimen ends in contact with compression platens.

Shear tests. Shear tests were performed on pure epoxy coupons in accordance with ASTM D5379 [35]. A CNC machine was used to obtain the V-notched beam test coupon. Prior to testing, a random graphite pattern was applied to measure the strains by DIC. The shear tests were carried out at 1 mm/min using an Instron™ UTS 5966 up to failure. The loading-rate was established at 1 mm/min.

2.3.2. Out of plane properties

Properties through the thickness. The thick unidirectional panel was manufactured to characterize the out of plane properties of the composite. The panel was sliced in the thickness direction using a wet diamond saw to obtain composite slices with the transverse direction representative of the thickness direction.

For tensile tests, slices were machined using a CNC machine. Due to the difficulty in manufacturing thick UD panels, coupon dimensions in the 1–3 plane were 100 × 20 × 3 mm^3, while those in the 2-3 plane were 200 × 20 × 3 mm^3. A biaxial strain gage was bonded to measure both longitudinal and transverse strains during the tensile tests. These measurements are needed to determine the out-of-plane Poisson ratios. The tensile tests were performed on an Instron™ 5966 machine with a 10 kN load cell at 1 mm/min.

For shear tests on composites, the ASTM standard D5379 was followed. Slices were machined using a CNC machine to obtain the V-notched beam test coupon. Prior to testing, a random graphite pattern was applied to measure the strains by DIC. The shear tests were carried out at 1 mm/min using an Instron™ 5966 machine up to failure and allowed the determination of G_{13} and G_{23} and the associated shear strengths. To saturate the thick composite in seawater it was first cut into 3 mm thick Iosipescu specimens before immersion for 4 months in seawater at 60 °C. Diffusion modeling indicated that this will result in saturation.

Interlaminar properties. Despite exceptional in-plane properties, the weakness of laminated composites is their low tolerance to delamination due to out-of-plane loading. To obtain a good description of the interface behavior and to predict the tolerance to delamination of a composite structure, fracture tests following different loading modes are needed [46]. Standard test procedures are available for Mode I [47], Mode II [48] and Mixed-Mode (I/II) fracture [49]. A previous study [33] provided a set of data for a similar material to the one presented here, but during that study the role of physical aging was not clearly defined. In the present study physical aging has been more closely controlled. During the fracture tests, images of specimen edges were taken continuously and were then post-processed to determine the crack tip position. Prior to testing, all coupons were pre-cracked in Mode-I at a loading-rate of 5 mm/min.

Pure Mode I tests. The Double Cantilever Beam (DCB) test method (ASTM D5528 [38]) was chosen in order to determine the Mode-I fracture toughness. Specimens were cut to dimensions of 20 × 195 mm^2. The Compliance Calibration (CC) data reduction method was used for calculating the value of pure Mode-I fracture toughness G_{Ic}. In this method, a least squares plot of $\log\left(\frac{\delta_i}{P_i}\right)$ vs. $\log(\boldsymbol{a_i})$ is generated, with $\boldsymbol{\delta_i}$ and $\boldsymbol{P_i}$ respectively the crosshead displacement and load, and $\boldsymbol{a_i}$ the visually observed delamination crack length at initiation. The slope is defined by a variable n, which is introduced in Eq. (5) to calculate G_I. The interlaminar fracture toughness corresponds to the average value of

experimental points on the plateau of the R curve (G_I versus crack length).

$$G_{IC} = \frac{nP\delta}{2ba} \tag{5}$$

Pure Mode II tests. The Calibrated End-Loaded Split (C-ELS) test method (ISO 15114 [39]) was chosen to determine the Mode-II fracture toughness as this configuration provides stable crack propagation. Specimens were cut to dimensions of 20 × 195 mm^2. A first step was performed to calibrate the flexural modulus of each coupon at free lengths of 50 mm, 60 mm, 70 mm, 80 mm and 90 mm. Once the initial slope (displacement/load) is known, it is possible to determine the flexural modulus using Eq. (6).

$$E_1 = \frac{1}{2b(h \times slope)^3} \tag{6}$$

Finally, the corrected beam theory using effective crack length is applied (Eq. (7)) and allows the determination of the Mode-II fracture toughness G_{IIC}. The interlaminar fracture toughness corresponds to the average value of experimental points on the plateau of the R curve.

$$G_{IIC} = \frac{9P^2a_e^2}{4b^2h^3E_1} \tag{7}$$

Mixed-Mode bending tests. The Mixed Mode bending method (ASTM D6671 [40]) was chosen to determine the mixed Mode I-Mode II fracture toughness. For this test, the contributions of both modes affect the crack propagation. A scheme representing the test is shown in Fig. 2. The mode ratio is determined using Eq. (8) from [50]. For this study, tests were performed at four levels of mode II contribution: 23%, 43%, 60% and 80%.

$$\frac{G_I}{G_{II}} = \frac{3(e+L)^2}{3(e+L)^2 + 4(3e-L)^2} \tag{8}$$

Calculations of fracture toughness need to consider both in-plane and out-of-plane properties by determining the crack length correction factor χ (Eqs. (9) and (10)). Values from experimental tests were chosen.

$$\Gamma = 1,18 \cdot \frac{\sqrt{E_{11} \cdot E_{22}}}{G_{13}} \tag{9}$$

$$\chi = \sqrt{\frac{E_{11}}{11 \cdot G_{13}} \cdot \left(3 - 2 \cdot \left(\frac{\Gamma}{1+\Gamma}\right)^2\right)} \tag{10}$$

Finally, mode I and mode II contributions to strain energy release rates were calculated from Eqs. (11) and (12). In these equations, P represents the load (N), c the lever length of the fixture (mm), L the half span length ($L = 68.7$ mm here), B and h respectively the width and the half thickness of the coupon and a the crack tip location (mm).

The introduction of these values allows the calculation of the mode mixture fracture toughness G_C using Eqs. (13) and (14).

$$G_I = \frac{12 \cdot P^2 \cdot (3c-L)^2}{16 \cdot b^2 \cdot h^3 \cdot L^2 \cdot E_{1f}} \cdot (a + \chi \cdot h)^2 \tag{11}$$

$$G_{II} = \frac{9 \cdot P^2 \cdot (c+L)^2}{16 \cdot b^2 \cdot h^3 \cdot L^2 \cdot E_{1f}} \cdot (a + 0,42 \cdot \chi \cdot h)^2 \tag{12}$$

$$G = G_I + G_{II} \tag{13}$$

$$\frac{G_{II}}{G} = \frac{G_{II}}{G_I + G_{II}} \tag{14}$$

Finally, G_C is determined from the average of fracture toughness values on the plateau of the R curve.

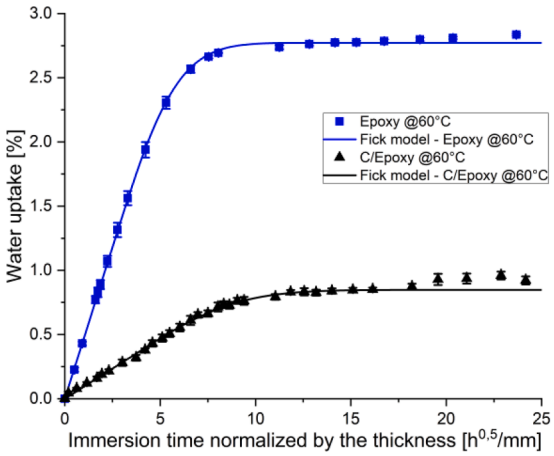

Fig. 3. Water uptake for pure Epoxy and quasi-isotropic coupons immersed in natural seawater at 60 °C for 8 months.

Table 2
Influence of aging on properties of epoxy resin.

	Rejuvenated	Physically aged	Seawater aged
Tensile stress at failure [MPa]	56.4 ± 0.6	79.5 ± 1.9	42.9 ± 0.3
Shear stress at failure [MPa]	45.5 ± 0.4	56 ± 2.7	33.7 ± 0.3

2.4. Flexural behavior tests

Four-point bending tests were performed on $[0,(-45,45)_2,90°]_S$ coupons in order to provide test data to compare to model predictions for unaged and aged specimens. The ASTM D6272 [42] standard was followed but the depth to span ratio was set at 12, to increase the out-of-plane shear contribution.

Finite element modeling of this test was performed using Abaqus™. The coupon was modeled using 8 nodes with reduced integration continuum shell elements (SC8R). The problem was solved using the explicit solver. More details are given below.

3. Results & discussion

First, results for water diffusion in the pure resin and the composite are presented. Then, the changes in the stiffness matrix and strengths with aging are discussed. Finally, the data obtained from the different tests were implemented in a numerical model to describe the flexural behavior before and after aging.

3.1. Diffusion kinetics

Fig. 3 shows the water uptake as a function of normalized immersion time. At saturation the epoxy absorbs 2.8% by weight, while the C/epoxy absorbs 0.85%. The difference is due to the fiber volume content of the composite supposing that the carbon fibers do not absorb water. At 60 °C, a saturation plateau is observed after an immersion time around 13 $\sqrt{h}.mm^{-1}$. This represents, for a thickness of 4.4 mm, an immersion time of 5 months. The immersions were continued for 8 months in order to check that a plateau had been reached.

3.2. Influence of aging on epoxy properties

Tensile and shear tests have been performed on pure (unreinforced) epoxy coupons in order to characterize the influence of aging on ultimate properties. Results are shown in Table 2. These clearly indicate that the resin is sensitive to both types of aging. Physical aging results in an increase in the tensile and shear stresses at failure of 41 and 23%

Table 3
Change of the in-plane mechanical properties with aging.

	Rejuvenated	Physically aged	Seawater aged
E_{11} [GPa]	127.54 ± 3.18	128.03 ± 4.45	128.41 ± 6.92
E_{22} [GPa]	7.94 ± 0.6	9.23 ± 0.78	4.39 ± 0.45
ν_{12} [-]	0.274 ± 0.010	0.320 ± 0.025	0.341 ± 0.026
G_{12} [GPa]	3.72 ± 0.12	4.07 ± 0.05	2.70 ± 0.08

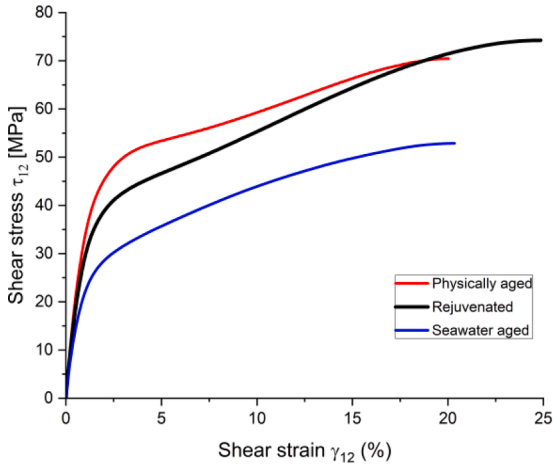

Fig. 4. Stress vs. strains plots of pure Epoxy coupons in tension before and after aging.

Table 4
In-plane stress at failure for 0°, ±45° and 90° oriented fibers with aging (*End tab failure).

	Rejuvenated	Physically aged	Seawater aged
X^T [MPa]	2271.7 ± 136.5	2140.3 ± 24.7	(1760 ± 96*)
X^C [MPa]	933.6 ± 50.1	949.9 ± 76.1	607 ± 33
Y^T [MPa]	38.3 ± 1.7	36.4 ± 5.5	16.6 ± 1.3
Y^C [MPa]	123.5 ± 4.2	134.2 ± 2.6	94.1 ± 3.4
S^T [MPa]	73.3 ± 3.0	68.7 ± 1.6	54.0 ± 1.0

respectively compared to the rejuvenated values. Seawater saturation results in a drop of 24 and 26%. It may be noted that such a result is common in the literature. For epoxies, when the only degradation phenomenon is plasticization, typical losses for both modulus and strength are around 20 to 25%.

3.3. Influence of aging on composite in-plane properties

All in-plane composite elastic properties except those in the fiber direction were affected by the seawater aging (Table 3). Unlike the

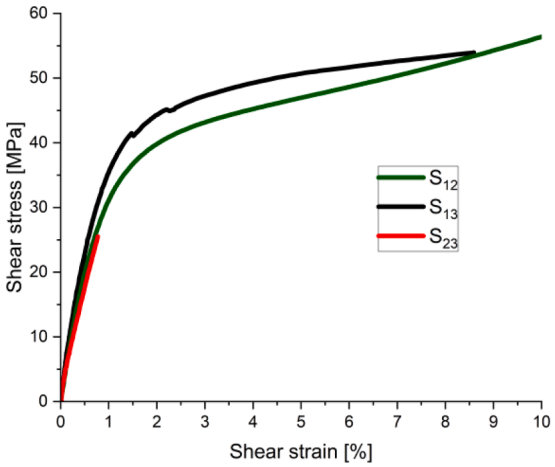

Fig. 6. Differences in Shear stress [MPa] vs. Shear strain [%] plots for rejuvenated coupons cut in the 12, 13 and 23 planes.

coupons of composite oriented at ±45° (Fig. 4), matrix dominated mechanical tests show improvements of the modulus with the physical aging and a decrease with the seawater aging. The influence of physical aging on the shear behavior has been investigated in the past [51]. In [45], the embrittlement of the epoxy during the physical aging was shown to result in the growth of microcracks at lower load, and as the toughness is also reduced, the growth of microcracks leads to global failure more quickly. With respect to the increase of the modulus, one explanation is that as the modulus is defined between 0.2% and 0.4%, the load is still low, and so the microcracks have not appeared yet. Thus, the modulus is calculated on an undamaged material, and this may be the reason why the modulus is higher after physical aging.

The last aspect considered is the change in ultimate ply properties after aging. Tension and compression tests have been performed on UD specimens in the 0° and 90° directions. Tension tests have also been performed on ±45° coupons to determine the shear stress at failure. Results are shown in Table 4. In tension, the physical aging tends to improve the stress at failure for both orientations while the seawater aging decreases it significantly. The influence of aging on compressive properties has previously been studied for open-hole compression [52]. In that study, the T800 carbon fiber-epoxy quasi-isotropic composite coupons were aged in humidity chambers at 70 °C and 85% RH for 40 days until the equilibrium weight gain was reached. The authors noted a loss of only 4% of the stress at failure.

For the seawater aging, the loss in compression strength is estimated to be 35% for 0° and 24% for 90°. For the 90° specimens, the failure starts in rich resin regions due to the inhomogeneity of the material at the mesoscale. For the 0° loading, as the compression is in the fiber direction, the loss was not expected to be so high. Two main aspects can explain this. First, it was stated earlier that the usual losses observed

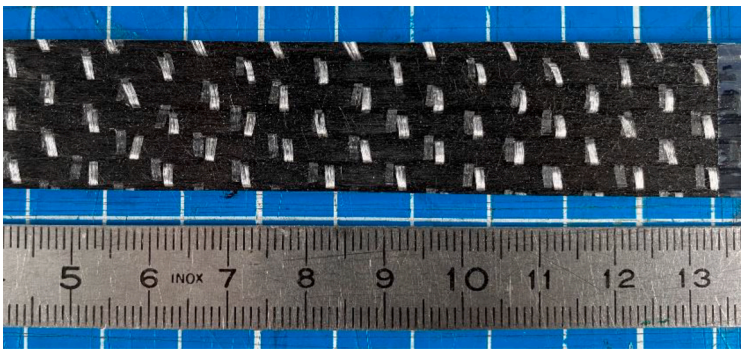

Fig. 5. Polyester weft threads added to maintain the carbon fiber yarn during manufacturing process.

Table 5
Out-of-plane shear properties of the C/Epoxy studied before and after aging.

	Rejuvenated	Physically aged	Seawater aged
G_{13} [GPa]	4.60 ± 0.17	5.17 ± 0.27	3.21 ± 0.17
G_{23} [GPa]	3.07 ± 0.12	3.02 ± 0.23	2.48 ± 0.28
τ_{13} [MPa]	43.4 ± 2.9	41.7 ± 3.0	25.8 ± 1.6
τ_{23} [MPa]	24.6 ± 2.2	21.2 ± 2.7	18.6 ± 1.3

Table 6
Out-of-plane Poisson's ratio of the C/Epoxy before and after aging.

	Rejuvenated	Physically aged	Seawater aged
ν_{13}	0.29 ± 0.01	0.32 ± 0.01	0.39 ± 0.01
ν_{23}	0.48 ± 0.01	0.48 ± 0.01	0.52 ± 0.01

after sea water aging are about 20 to 25%. When the loss is higher, it usually suggests that the interface may have been degraded. This will be further discussed later. The second reason is the presence of weft stitching (Fig. 5). Carbon fibers in the warp direction are deviated by the presence of these polyester weft threads, and the main consequence is a reduced compression resistance [53] due to fiber misalignment, in contrast with the straight fibers in a prepreg-based composite. After seawater aging, the properties of the matrix drop due to water ingress in the material. Swelling of the stitching during immersion may also contribute to the loss in strength. In all cases, failure occurred in the gage section.

3.4. Influence of aging on composite out-of-plane properties

Fig. 6 shows the shear stress as a function of shear strain plotted for a rejuvenated coupon cut in the 13 and 23 planes. The failure modes are quite different (Fig. 7) since the shear plane is normal to the fiber direction in one case (1) and parallel to the fiber direction in the other case (2) where it leads to a brittle failure. For the shear test in 13 direction, irregularities are noted on Fig. 6 and correspond to matrix cracking in the V-notched part of the coupon.

Changes to out-of-plane shear modulus and shear stress at failure after aging are shown in Table 5. With respect to the reference state, the seawater aging reduces both modulus values, while only G_{13} is affected by the physical aging. Because of the nature of the Iosipescu coupons, values of τ_{13} were determined at the first load drop. For seawater aged coupons all values are significantly lower than those for unaged specimens.

Results for Poisson's ratios are shown in Table 6. Compared to the rejuvenated state, the physical aging increases all Poisson's ratios. A value of $\nu_{23} > 0.5$ was measured after seawater aging. While this value is not possible for isotropic materials, higher values have been measured experimentally in the past [54,55] on orthotropic materials. However, the presence of porosity in these specimens taken from the thick plate may also affect this result.

3.5. Influence of aging on crack propagation

Another aspect studied here is the influence of aging on delamination. Crack propagation tests were performed for different mode I, mode II and mixed-mode ratios to characterize the damage propagation at the mid-plane interface.The influence of the mode ratio on the propagation fracture toughness is shown in Fig. 8. No significant change is seen between the rejuvenated and the physically aged states. However, the seawater aging appears to reduce the fracture toughness when the Mode-II ratio increases. For the pure Mode-II fracture test, SEM observations are shown in Fig. 9. At the same magnification, we can observe large hackles for the seawater aged coupons and smaller hackles for the physically aged coupons. These conclusions are corroborated by the tensile tests on pure epoxy coupons, for which a brittle fracture was noted after physical aging and a ductile fracture after seawater aging.

Table 7
Mixed-mode fracture toughness values and fit parameter for the BK criterion.

	Rejuvenated	Physically aged	Seawater aged
G_{IC} [kJ/m^2]	0.63 ± 0.06	0.60 ± 0.06	0.50 ± 0.06
G_{IIC} [kJ/m^2]	1.46 ± 0.09	1.46 ± 0.24	1.04 ± 0.14
η	1.59	1.67	0.58

Table 8
Experimental values normalized with the rejuvenated and dried state (reference).

	Property considered	Physically aged [PA]	Seawater aged [SWA]
Design properties	E_{11} [-] *	1.08	1.01
	E_{22} [-]	1.16	0.55
	E_{33} [-]	–	–
	ν_{12} [-] *	1.17	1.24
	ν_{13} [-] *	1.12	1.33
	ν_{23} [-] *	1.01	1.08
	G_{12} [-]	1.09	0.73
	G_{13} [-]	1.12	0.70
	G_{23} [-]	0.98	0.81
Ply properties	Xt [-]	0.94	0.77
	Xc [-]	1.02	0.65
	Yt [-]	0.95	0.43
	Yc [-]	1.09	0.76
	S_{12} [-]	0.94	0.74
	S_{13} [-]	0.96	0.59
	S_{23} [-]	0.86	0.76
Interface properties	Matrix tension [-]	1.41	0.76
	Matrix shear [-]	1.23	0.74
	G_{Ic} [-]	0.95	0.79
	G_{IIc} [-]	1.00	0.71
	n [-] *	1.05	0.36
Average		+ 5%	- 30%

Results concerning the sea water aged samples were also quite surprising. In the literature, it has been demonstrated several times that water ingress can increase the fracture toughness value because of plasticization. Here again, a degradation of the interface may explain the results shown here.

For modeling the change of the fracture toughness with mode ratio, the B-K criterion proposed by Benzeggagh and Kenane was applied [56]. The equation of the model is shown in Eq. (15). The values of G_{Ic}, G_{IIc}, and the fitting parameter η are presented in Table 7.

$$G_T = G_{Ic} + (G_{IIc} - G_{Ic})\left(\frac{G_{II}}{G}\right)^{\eta} \quad (15)$$

3.6. Normalization of property changes with the aging

For each property determined experimentally, a normalization with respect to the rejuvenated state (reference) is applied, as summarized in Table 8. This provides a global view of the property changes due to aging. Properties that are not used for the calculation of the influence of aging in the Table are marked with an asterisk (*). The separation was performed because it is not expected that the fiber behavior will be affected by the aging until damage is observed.

The average change in the mechanical properties after physical aging is a 5% increase, whereas an average loss of 30% was found after seawater aging.

3.7. Application of aged properties to flexural behavior prediction

3.7.1. Experimental tests

To examine the use of this set of data in a practical application, three sets of quasi-static 4-point flexural tests were performed, on reference and aged quasi-isotropic specimens. The standard ASTM D6272 was

followed. The test geometry used is an intermediate loading condition, between a short beam test dominated by interlaminar shear (L/t = 5) and a long beam test (L/t = 24) closer to pure flexure. A span to thickness ratio of L/t = 12 was chosen. The configuration of one third was chosen between the load span and the support span. The loading-rate was 1 mm/min and 3D digital image correlation was performed to measure the beam displacement throughout the test. In each case samples were tested in the rejuvenated, physically aged and seawater saturated conditions. The tests were carried out until coupon failure. The failure occurs at the same stress for both rejuvenated and physically aged states, but it is reduced by 36% after seawater aging. The physical aging reduces the non-linearity before the failure in comparison with the rejuvenated state, the failure is more brittle after physical aging.

The 3D digital image correlation shows the difference in damage a few seconds before the coupon failure (Fig. 10). In all cases, the failure was located between the mobile and the static support points. In the case of rejuvenated and physically aged coupons, the damage seems to be local and then propagates abruptly leading to the global failure. For seawater aged coupon, damage is more distributed. In addition, on the upper face of the seawater aged coupons where compressive strains are measured, fiber bundles were observed to break.

3.7.2. Numerical simulation

A numerical simulation of this experimental test was performed with the commercial finite element solver Abaqus™ Explicit, Fig. 11. Plies were modeled individually using continuum shell elements (SC8R) and were stacked using cohesive surfaces. The material input data were therefore limited to the in-plane data, but the characterization described above would enable a full 3D model to be applied. A linear elastic traction-separation behavior has been defined with Knn=24,600 N/mm^3, Kss=Ktt=14,200 N/mm^3. The load was applied by discrete rigid rollers with a radius of 5 mm, meshed with R3D4 elements. The friction coefficient between the material and the pins was defined to be 0.05. The material constitutive model [57] was based on Hashin's failure criteria for unidirectional fiber composites [58]. This model is included in the Abaqus™ library. The experimental failure in the upper ply was observed to be at the fiber yarn scale. A preliminary mesh sensitivity study was performed with dimensions of 0.5, 1, 1.5 and 3 mm, and the stiffness did not change when the mesh was smaller than 1.5 mm. The mesh dimensions were therefore chosen to have a mesh width equal to 1.5 mm, which represents two elements in the yarn width. A relatively high loading rate (0.2 m/s) was needed because of the explicit method. A smooth step was used to apply the load gradually. The balance of energy has been checked [57] to verify inertia effects, and this loading rate did not induce significant dynamic effects on the simulation results.

3.7.3. Intralaminar and translaminar fracture toughness properties

In the Abaqus™ model, crack propagation values are needed to consider the energy released when translaminar and intralaminar cracks propagate. It was not possible to obtain valid experimental data for translaminar cracking due to premature failure in compression tests on CC and CT coupons. The mode I and II translaminar fracture toughness prior to aging have therefore been taken from a published study [59]. A reference value of 60 kJ/m^2 has been used for the rejuvenated material, and the comparison with the experimental results shows reasonable agreement with this assumption for this state. To correctly capture the force at failure for the seawater saturated material a reduction to 40 kJ/m^2 was necessary, and an increase to 80 kJ/m^2 was found to be suitable for the physically aged state. A comparison between a seawater saturated coupon test and simulations with different values of translaminar fracture toughness is presented in Fig. 12.

The third fracture toughness values required are intralaminar. Very few studies have considered the intralaminar fracture toughness [60] mainly due to the lack of standard test methods. These properties are therefore generally assumed to have the same values as the interlaminar fracture toughness [61], determined using DCB, ELS and MMB test

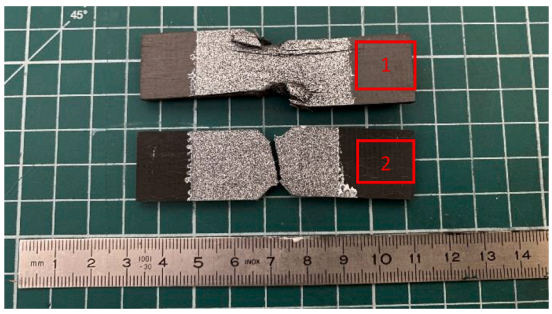

Fig. 7. Rejuvenated coupons after shear test (1) in 1–3 and (2) in 2–3 planes.

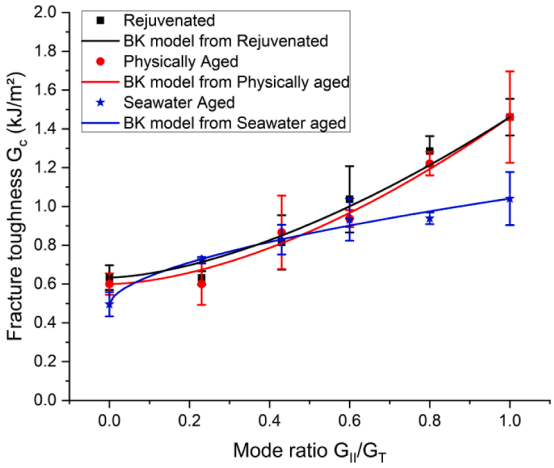

Fig. 8. Change of the propagation fracture toughness with the mode ratio (from left to right: rejuvenated, physically aged and seawater aged).

methods. This assumption is commonly made since interlaminar and intralaminar fracture both involve matrix plasticity and degradation, and fiber-matrix interfacial debonding. For prepreg materials, this assumption makes sense, because of the material homogeneity at mesoscale. However, in the present study, weft stitching is likely to improve the intralaminar tensile fracture toughness. For the intralaminar compressive fracture toughness, no studies have been found. The mode I and II intralaminar fracture toughness are here supposed to be equal to the interlaminar fracture toughness, Table 10.

3.7.4. Comparison experiment / simulation

Fig. 13 shows the predicted and the experimental responses of the four-point bending test. As expected, there is a significant influence of seawater saturation on the flexural response. The flexural model captures the coupon failure level and the stiffness quite well. For the rejuvenated material, a nonlinear behavior is observed experimentally but not well predicted. This may be due to the type of element chosen, which does not consider out-of-plane damage. Stiffness and stress at failure are compared respectively in Tables 11 and 12. The stiffness and the failure loads are slightly over-estimated by the model, but the differences are small, and may be due to variations in the ply thickness. This exercise shows that it is essential to include seawater aging data in design of immerged structures. In this simple application thin composites are tested but for thicker materials the coupling with a water diffusion model would enable a gradual change in properties to be integrated, as saturation will take much longer (Figs. 7, 8, 13, Table 9).

4. Conclusion

In this study, in-plane and out-of-plane properties of a C/Epoxy composite manufactured by infusion have been characterized for three

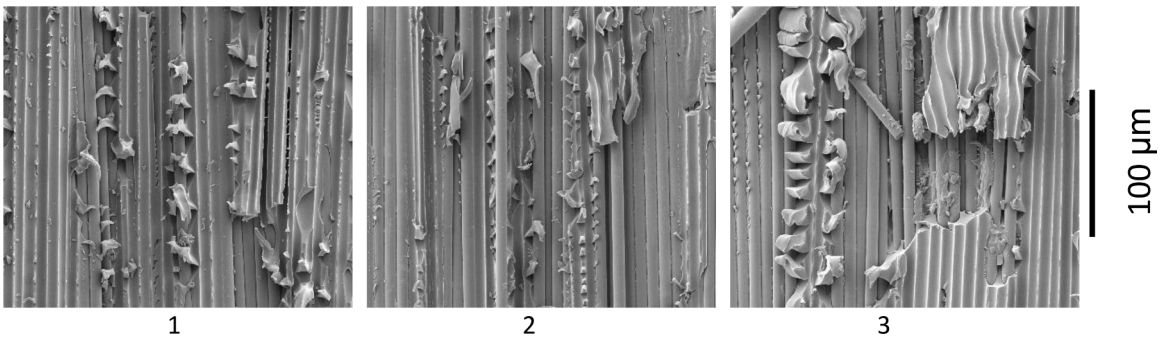

Fig. 9. Comparison between the interfacial fracture pattern for pure Mode-II test for (1) Rejuvenated, (2) Physically Aged and (3) Seawater aged (hackles).

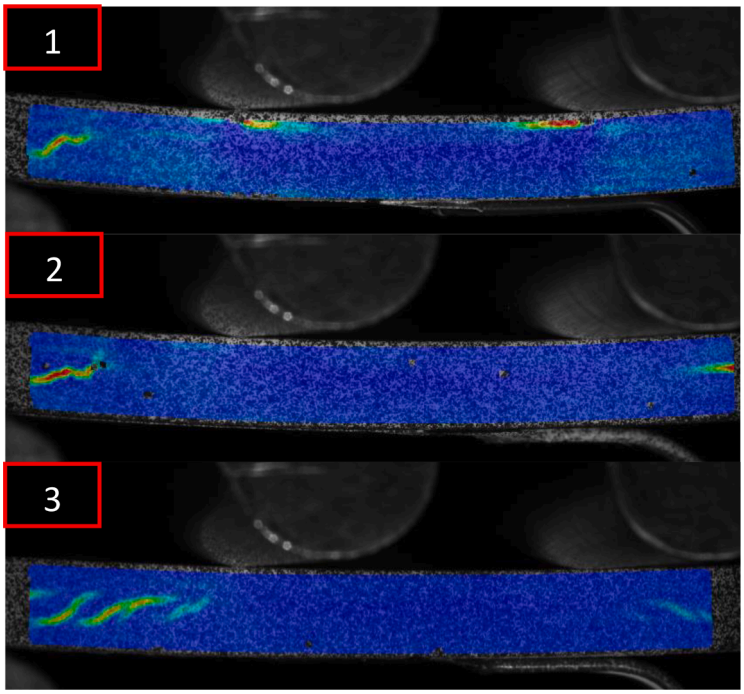

Fig. 10. Major strain computed by 3D DIC of four point bending coupon a few seconds before the failure. From top to bottom: (1) Rejuvenated, (2) Physically aged and (3) Seawater aged.

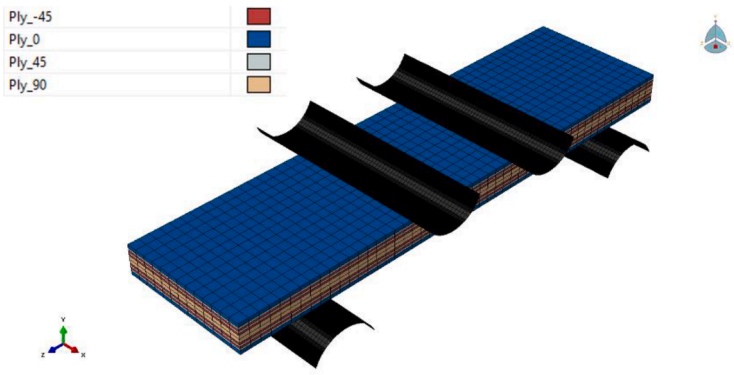

Fig. 11. Numerical model of the four-point bending test.

aging states: dried and rejuvenated (without physical aging), physically aged, and seawater aged to saturation. It was demonstrated that physical aging had, in most cases, a beneficial effect on the mechanical properties used in design, while seawater aging results in a reduction in stiffness and strength. The latter is significant, and must be considered in design of marine structures. In terms of interlaminar crack propagation, significant seawater aging effects were noted for in-plane shear (mode II) loadings, for which a reduction of G_{IIc} by 30% was measured. The reference, physically aged and seawater aged properties were introduced in numerical simulations of four point bending tests combining

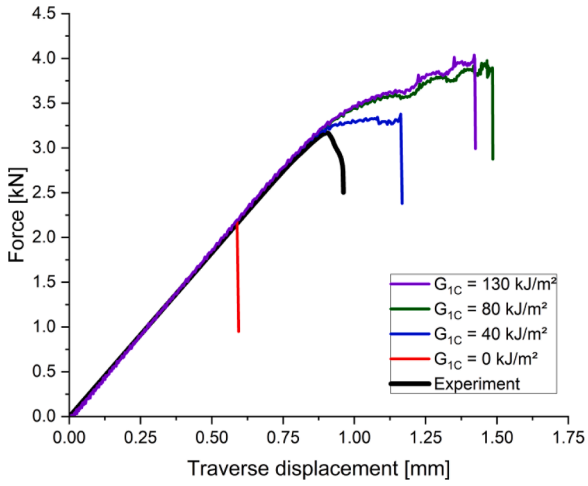

Fig. 12. Comparison of Force-Displacement curves for 4-point flexure tests on seawater saturated coupon with model predictions using different values of translaminar G_{1C} (FE mesh = 1.5 mm).

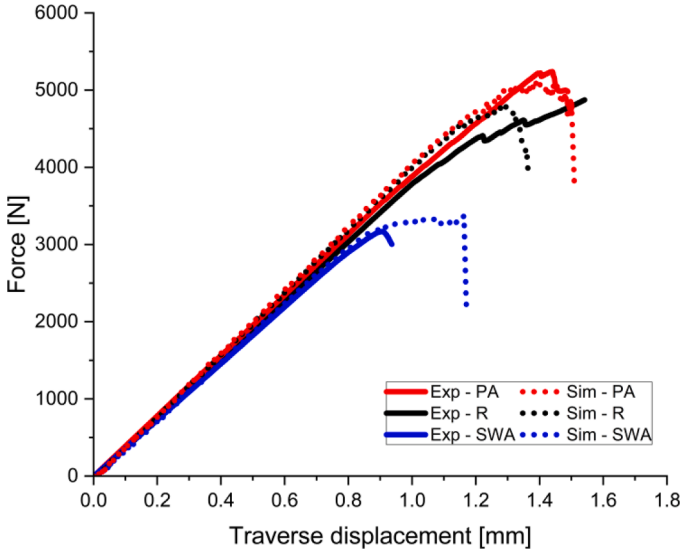

Fig. 13. Comparison between experiment and simulation of the 4 point bending test for 3 conditions.

Table 9
Influence of the aging on the flexural stress at failure.

	Rejuvenated	Physically aged	Seawater aged
Flexural stress at failure [MPa]	620 ± 22	631 ± 27	400 ± 8

Table 10
Properties used for translaminar and intralaminar damage propagation.

	Rejuvenated	Physically aged	Seawater aged
G_{IC}^{Ten} [kJ/m^2] (Trans)	60	80	40
G_{IC}^{Comp} [kJ/m^2] (Trans)	60	80	40
G_{IIC}^{Ten} [kJ/m^2] (Intra)	0.63	0.60	0.50
G_{IIC}^{Comp} [kJ/m^2] (Intra)	1.46	1.46	1.04

flexure and shear loads, and a good prediction of the unaged and aged behavior was obtained. The study also highlighted a lack of reliable input data for translaminar and intralaminar fracture, and development of test methods for these properties would improve confidence in numerical modeling of composite structures.

Table 11
Comparison between experimental and numerical bending stiffness.

	Rejuvenated	Physically aged	Seawater aged
Experimental [N/mm]	3808 ± 69	3886 ± 159	3645 ± 16
Numerical [N/mm]	4074	4101	3806
Difference [%]	*7*	*5*	*4*

Table 12
Comparison between experimental and numerical bending stress at failure.

	Rejuvenated	Physically aged	Seawater aged
Experimental [MPa]	619.8 ± 21.5	631.1 ± 26.6	400.1 ± 8.2
Numerical [MPa]	652.8	696.2	456.0
Difference [%]	*5*	*9*	*12*

Declaration of Competing Interest

The authors declare that they have no known competing financial interests or personal relationships that could have appeared to influence the work reported in this paper.

Data availability

The authors do not have permission to share data.

References

[1] J. Graham-Jones, J. Summerscales, Marine Applications of Advanced Fibre-Reinforced Composites, Elsevier, 2016. Woodhead Publishing Series in Composites Science and Engineering.
[2] A.P. Mouritz, E. Gellert, P. Burchill, K. Challis, Review of advanced composite structures for naval ships and submarines, Compos. Struct. 53 (1) (2001) 21–42. Jul.
[3] D.W. Chalmers, The properties and uses of marine structural materials, Mar. Struct. 1 (1) (1988) 47–70. Jan.
[4] L.S. Sutherland, A review of impact testing on marine composite materials: part I – Marine impacts on marine composites, Compos. Struct. 188 (2018) 197–208. Mar.
[5] C.R. Kennedy, S.B. Leen, C.M. Brádaigh, A preliminary design methodology for fatigue life prediction of polymer composites for tidal turbine blades, Proc. IMechE 226 (3) (2012) 203–218. Jul.
[6] A.G.L. Borthwick, Marine renewable energy seascape, Engineering 2 (1) (2016) 69–78. Mar.
[7] G. Dolo, S. Durand, F. Boursier, P. Muller, F.Le Lay, Composite propeller in marine industry: first steps toward a technological breakthrough, in: Proceedings of the *OCEANS*, Marseille, 2019, pp. 1–6. Jun.
[8] A.F. Molland, S.R. Turnock, The design and construction of model ship propeller blades in hybrid composite materials, Compos. Manuf. 2 (1) (1991) 39–47. Mar.
[9] T.J. Searle, J. Chudley, D. Short, Composites offer advantages for propellers, Reinf. Plast. 37 (12) (1993) 24–26. Dec.
[10] C.C. Lin, Y.J. Lee, C.S. Hung, Optimization and experiment of composite marine propellers, Compos. Struct. 89 (2) (2009) 206–215. Jun.
[11] K. Beng Yeo, W.J. Leow, W.H. Choong, F. Mohd Tamir, Hand lay-up GFRP composite marine propeller blade, J. Appl. Sci. 14 (22) (2014) 3077–3082. Dec.
[12] B.-G. Paik, et al., Investigation on the performance characteristics of the flexible propellers, Ocean Eng. 73 (2013) 139–148. Nov.
[13] P. Maung, B.G. Prusty, J.M. White, M. David, A.W. Phillips, N.A. St John, Structural performance of a shape-adaptive composite hydrofoil using automated fibre placement, Eng. Struct. 183 (2019) 351–365. Mar.
[14] J.M. White, P. Maung, M. David, A.W. Phillips, N.A. St John, B.G. Prusty, Hydrofoil manufacture with automated fibre placement, in: Proceedings of the *9th Australasian Congress on Applied Mechanics (ACAM9)*, 2017, p. 773.
[15] P. Davies, Y.D.S. Rajapakse, Durability of Composites in a Marine Environment, Springer Netherlands, Dordrecht, 2014, 208.
[16] P. Davies, Y.D.S. Rajapakse, Durability of Composites in a Marine Environment 2, Springer International Publishing, Cham, 2018, 245.
[17] J.D. Garcia-Espinel, D. Castro-Fresno, P.Parbole Gayo, F. Ballester-Muñoz, Effects of sea water environment on glass fiber reinforced plastic materials used for marine civil engineering constructions, Mater. Des. 66 (2015) 46–50. *1980-2015*Feb.
[18] L.S. Sutherland, A review of impact testing on marine composite materials: part II – Impact event and material parameters, Compos. Struct. 188 (2018) 503–511. Mar.

[19] H. Matos, C. Javier, J. LeBlanc, A. Shukla, Underwater nearfield blast performance of hydrothermally degraded carbon–epoxy composite structures, Multiscale Multidiscip. Model. Exp. Des. 1 (1) (2018) 33–47. Mar.
[20] C. Javier, H. Matos, A. Shukla, Hydrostatic and blast initiated implosion of environmentally degraded Carbon-Epoxy composite cylinders, Compos. Struct. 202 (2018) 897–908. Oct.
[21] D. Fontaine, J. LeBlanc, A. Shukla, Blast response of carbon-fiber/epoxy laminates subjected to long-term seawater exposure at sea floor depth pressures, Compos. Part B Eng. 215 (2021), 108647. Jun.
[22] T. Chu, D. Fontaine, J. LeBlanc, A. Shukla, Collapse behavior of carbon-fiber epoxy cylinders subjected to long-term seawater exposure at seafloor depth pressures, Mar. struct. 84 (2022), 103219. Jul.
[23] D.E. Walrath, D.F. Adams, The losipescu shear test as applied to composite materials, Exp. Mech. 23 (1) (1983) 105–110. Mar.
[24] D.O. Adams, J.M. Moriarty, A.M. Gallegos, D.F. Adams, The V-Notched Rail Shear Test, J. Compos. Mater. 41 (3) (2007) 281–297. Feb.
[25] J.Y. Cognard, L. Sohier, P. Davies, A modified Arcan test to analyze the behavior of composites and their assemblies under out-of-plane loadings, Compos. Part A 42 (1) (2011) 111–121. Jan.
[26] R.F. Ferguson, M.J. Hinton, M.J. Hiley, Determining the through-thickness properties of FRP materials, Compos. Sci. Technol. 58 (9) (1998) 1411–1420. Sep.
[27] Y.T. Li, X.T. Zheng, G. Luo, A novel testing method for measuring through-thickness properties of thick composite laminates, KEM 525–526 (2012) 381–384. Nov.
[28] M.J. Laffan, Testing the toughness of polymer matrix composites. Failure Mechanisms in Polymer Matrix Composites, Elsevier, 2012, pp. 110–128.
[29] N. Tual, N. Carrere, P. Davies, T. Bonnemains, E. Lolive, Characterization of sea water ageing effects on mechanical properties of carbon/epoxy composites for tidal turbine blades, Compos. Part A (2015) 380–389. Nov. 01,.
[30] E. José-Trujillo, C. Rubio-González, J. Rodríguez-González, Seawater ageing effect on the mechanical properties of composites with different fiber and matrix types, J. Compos. Mater. 53 (23) (2019) 3229–3241. Sep.
[31] A. Le Guen-Geffroy, Marine ageing and fatigue of carbon/epoxy composite propeller blades, PhD Thesis, Université de Bretagne Occidentale, 2019.
[32] F. Ascione, L. Granata, L. Guadagno, C. Naddeo, Hygrothermal durability of epoxy adhesives used in civil structural applications, Compos. Struct. 265 (2021), 113591. Jun.
[33] A. Le Guen-Geffroy, P. Davies, P.Y. Le Gac, B. Habert, Influence of seawater ageing on fracture of carbon fiber reinforced epoxy composites for ocean engineering, Oceans 1 (4) (2020) 198–214. Sep.
[34] ISO 527-2 : Plastics. Determination of tensile properties: test conditions for moulding and extrusion plastics, BSI British Standards, 2023.
[35] ASTM D5379 : Test method for shear properties of composite materials by the V-notched beam method, ASTM International, 2023.
[36] ISO 527-5 : Plastics - determination of tensile properties: test conditions for unidirectional fibre-reinforced plastic composites, BSI British Standards, 2023.
[37] ASTM D6641 : Test method for compressive properties of polymer matrix composite materials using a combined loading compression (CLC) test fixture, ASTM International, 2023.
[38] ASTM D5528 : Test method for Mode I interlaminar fracture toughness of unidirectional fiber-reinforced polymer matrix composites, ASTM International, 2023.
[39] ISO/TC 61/SC 13, ISO 15114 : Fibre-reinforced plastic composites - determination of the Mode II fracture resistance for unidirectionally reinforced materials using the calibrated end-loaded split (C-ElS) test and an effective crack length approach test method for Mode I interlaminar fracture toughness of unidirectional fiber-reinforced polymer matrix composites, 2023.
[40] ASTM D6671 : Test method for mixed Mode I-Mode II interlaminar fracture toughness of unidirectional fiber reinforced polymer matrix composites, ASTM International, 2023.
[41] ASTM D3518 : Test method for in-plane shear response of polymer matrix composite materials by tensile test of a 45 Laminate, ASTM International, 2023.
[42] ASTM D6272 : Test method for flexural properties of unreinforced and reinforced plastics and electrical insulating materials by four-point bending, ASTM International, 2023.
[43] L.C.E. Struik, Physical Aging in Amorphous Polymers and Other Materials, Elsevier Science, 1977.
[44] C.G. Sell, G.B. McKenna, Influence of physical ageing on the yield response of model DGEBA/poly(propylene oxide) epoxy glasses, Polymer 33 (10) (1992) 2103–2113. Jan.
[45] G.M. Odegard, A. Bandyopadhyay, Physical aging of epoxy polymers and their composites, J. Polym. Sci. Part B Polym. Phys. 49 (24) (2011) 1695–1716.
[46] P. Davies, Introduction to delamination fracture of continuous fibre composites, in: European Structural Integrity Society, 28, Elsevier, 2001, pp. 271–275.
[47] A.J. Brunner, B.R.K. Blackman, P. Davies, Mode I delamination, in: European Structural Integrity Society, 28, Elsevier, 2001, pp. 277–305.
[48] P. Davies, B.R.K. Blackman, A.J. Brunner, Mode II delamination, in: European Structural Integrity Society, 28, Elsevier, 2001, pp. 307–333.
[49] B.R.K. Blackman, A.J. Brunner, P. Davies, Delamination fracture of continuous fibre composites: mixed-mode fracture, in: European Structural Integrity Society, 28, Elsevier, 2001, pp. 335–359.
[50] M. Kenane, M.L. Benzeggagh, Mixed-mode delamination fracture toughness of unidirectional glass/epoxy composites under fatigue loading, Compos. Sci. Technol. 57 (5) (1997) 597–605.
[51] E.S.W. Kong, Physical aging in epoxy matrices and composites. *Epoxy Resins and Composites IV*, Springer Berlin Heidelberg, Berlin, Heidelberg, 1986, pp. 125–171, 80K. Dušek, Ed.
[52] L. Xu, Y. He, S. Ma, L. Hui, Y. Jia, Y. Tu, Effects of aging process and testing temperature on the open-hole compressive properties of a carbon fiber composite, High Perform. Polym. 32 (6) (2020) 693–701. Aug.
[53] J.R. Reeder, Stitching vs. a toughened matrix: compression strength effects, J. Compos. Mater. 29 (18) (1995) 2464–2487. Dec.
[54] B.M. Lempriere, Poisson's ratio in orthotropic materials, AIAA J. 6 (11) (1968) 2226–2227. Nov.
[55] R.M. Jones, Mechanics of Composite Materials, 2nd ed., CRC Press, 2018.
[56] M.L. Benzeggagh, M. Kenane, Measurement of mixed-mode delamination fracture toughness of unidirectional glass/epoxy composites with mixed-mode bending apparatus, Compos. Sci. Technol. 56 (4) (1996) 439–449. Jan.
[57] Dassault Systemes, Abaqus documentation. 2022.
[58] Z. Hashin, Failure criteria for unidirectional fiber composites, J. Appl. Mech. 47 (2) (1980) 329–334. Jun.
[59] N. Blanco, D. Trias, S.T. Pinho, P. Robinson, Intralaminar fracture toughness characterisation of woven composite laminates. Part II: experimental characterisation, Eng. Fract. Mech. 131 (2014) 361–370. Nov.
[60] S.T. Pinho, P. Robinson, L. Iannucci, Developing a four point bend specimen to measure the mode I intralaminar fracture toughness of unidirectional laminated composites, Compos. Sci. Technol. 69 (7–8) (2009) 1303–1309. Jun.
[61] L.F. Varandas, D. Dalli, G. Catalanotti, B.G. Falzon, Estimating the mode I through-thickness intralaminar R -curve of unidirectional carbon fibre-reinforced polymers using a micromechanics framework combined with the size effect method, Compos. Part A 162 (2022), 107141. Nov.